Preprint 22-063

EVALUATION OF PARAMETERS INFLUENCING POTENTIAL GAS FLOW TO THE MINE IN THE EVENT OF A NEARBY UNCONVENTIONAL SHALE GAS WELL CASING BREACH

K. M. Ajayi, CDC NIOSH, Pittsburgh PA
Z. Khademian, CDC NIOSH, Pittsburgh PA
S. J. Schatzel, CDC NIOSH, Pittsburgh PA

ABSTRACT

The integrity of unconventional shale gas well casings positioned in the abutment pillar of a longwall mine could be jeopardized by longwall-induced deformations. Under such scenarios, the surrounding fracture networks could provide pathways for gas flow into the mine creating safety concerns. To provide recommendations for developing guidelines that ensure a safe co-existence of longwall mining and unconventional shale gas production, this study evaluates the impact of parameters that could affect potential shale gas flow into the mine in the event of a casing breach using a discrete fracture network (DFN) model. These parameters are evaluated using a conceptualized DFN realization that is representative of the fractured zone in the overburden, and the range of parameter variations are within values validated with field measurements. The results show that a decrease in fracture aperture (potentially due to longwall-induced stress in the likely vicinity of the breach location) reduces the potential gas flow to the mine by a significantly higher proportion. A 50% decrease in the aperture of the fracture that directly transports the gas from the casing breach location reduces the gas flow to the mine by over 70%. Similarly, changes in the fracture water saturation level significantly affect the gas flow. In all cases, the potential gas flow to the mine is higher if the casing breach occurs at an increased gas well pressure. These findings provide critical information regarding the impact of each of the parameters associated with gas flow in the event of a shale gas casing breach near a longwall mine and could help towards the development of guidelines to ensure a safe coexistence of both industries.

INTRODUCTION

Due to the recent boom in the U.S. energy industry, there has been a significant increase in the number of shale gas wells in Pennsylvania, West Virginia, Ohio, Virginia, and Tennessee. Though these wells are targeting the Marcellus shale resource at depths varying from 1,500–2,700 m [1], they penetrate through different coal seams at shallower depths. Figure 1 illustrates a mine site coexisting with shale gas well production in Southwestern Pennsylvania. As shown in Figure 1, the shale gas well penetrates through the two coal seams in the overburden and the Pittsburgh coal seam mining horizon. At the mining horizon, it is required that the gas well casing be protected by a coal pillar as illustrated in Figure 1 [2]. From the longwall mines data in Pennsylvania, mining depths in these regions could vary from about 94.49 m to 365.76 m (310 to 1,200 ft) [3]. In Belmont County, Ohio, most Pittsburgh coal bed occurrences are within 304.80 m (1,000 ft) from the surface [4]. Over the next 10 years, many shale gas wells will be mined by the Pittsburgh Seam longwalls. Though coal mining and conventional natural gas production have coexisted for many years, these unconventional wells are characterized with significantly higher-pressure gas. This presents a new array of concerns as mining could jeopardize the integrity of the casings, which could lead to the release of high-pressured gas into the overburden. The original guidance in Pennsylvania for protecting gas wells in pillars predated longwall mining in the United States [2].

On this subject, the Pennsylvania Department of Environmental Protection (PADEP) initiated a call for research to update the gas well pillar regulation. Consequently, researchers from the National Institute for Occupational Safety and Health (NIOSH) have been assessing the impact of longwall-induced deformation on gas wells near longwall mines with the intent of providing research-based evidence to prevent gas well casing integrity failure. The most likely locations identified for a casing breach are along the strong-to-weak rock interfaces present at 0–10 m below the mine floor and 0–30 m above the mine roof [1]. Similarly, the pillar yield and peak abutment pressure zone could affect the gas well casing if the distance between the casing and the edge of the gob is within 15.24 m (50 ft). In the event of an integrity failure, high-pressure gas from the casing is released in the overburden and could flow through the nearby fracture network towards the mine. This could increase the risk of a mine explosion or accumulation of methane beyond the mandated limits.

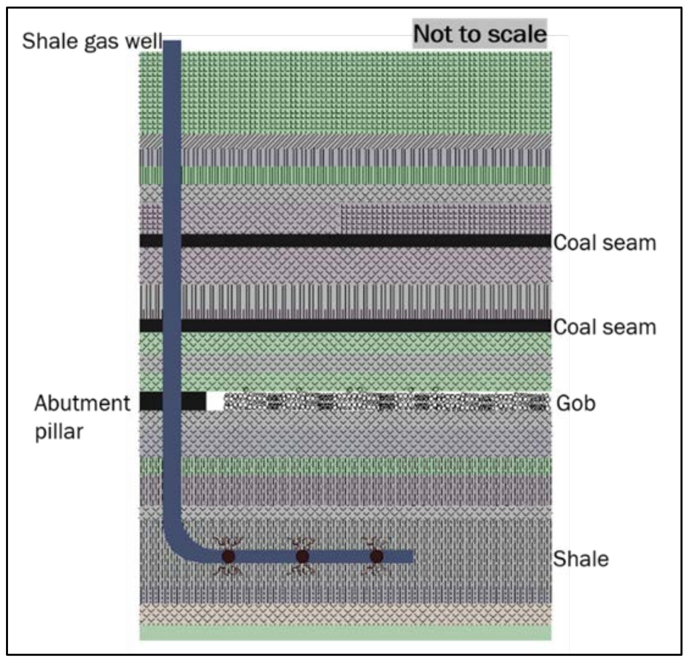

Figure 1. Schematic of a shale gas well casing positioned in the abutment pillar of a longwall mine showing the penetration of multiple coal seams.

The likelihood of gas flow from the breach location is dependent on the permeability of surrounding strata, which could be highly dependent on the in-situ and mining-induced fractures along with pore spaces in the rock matrix. Schatzel et al. [5] observed that permeability could increase by 100 to 500 times due to undermining, which could imply an increase of hundreds or thousands millidarcy depending on the site. It is also likely that the permeability could continue to change up to 7 months after mining [5]. These observations are mostly related to the strata response to tension and compression due to mining-induced deformation, which leads to the formation of the caved zone, fractured zone, and continuous deformation zone in the gob above the extracted coal. The fractured zone provides channels for the gas transport, and their permeabilities could be orders of magnitude higher than the rock matrix [6]. Therefore, gas transport through fractured rocks is predominantly through the fractures with the assumption that the rock matrix permeability is negligible. Consequently, numerical modeling using a discrete fracture network (DFN) model is often used to predict gas flow through fractured rocks. In most cases, it is unrealistic to deterministically characterize all the fracture parameters from a site. Hence, fracture models are often stochastic with incorporation of site data such as fracture sets, orientation, spacing, aperture, and fracture heights. On this project, Ajayi et al. [7] developed a stochastic DFN model to predict mining-induced permeability based on core log data from a site in southwestern Pennsylvania and validated the model with field measurements as summarized in Watkins et al. [8]. The aperture values for the stochastic DFN model were obtained from a geomechanical model conducted for the study site by Khademian et al. [9] and used to predict potential gas flow to the mine from a breached shale gas well casing. Their findings provided a distribution of gas flow based on the statistical distributions of the parameters, such as fracture aperture, fracture length, fracture location, and fracture orientation. The intent of using a stochastic approach is to model the effects of potential variation in fracture parameters in the overburden.

For example, fracture aperture varies at different heights based on the pre-mining, during-mining, and post-mining strata responses. A previous study observed that apertures in a shallow longwall mine could range from near zero to 1 m, depending on the location and orientation of the fractures with respect to the longwall panels [9]. Before mining, bedding plane apertures were generally at a higher level than the subvertical fractures, mainly due to the higher horizontal stresses with a horizontal-to-vertical stress ratio of 3. Apertures of all fractures at the center of the panel were minimal because of high lateral and vertical compaction due to the caving process and bending of overburden layers. Minimum aperture values were also shown above abutment pillars because of the longwall-induced pillar stress concentration after mining the panels. The maximum apertures in all fractures were observed at the edge of panels due to bedding plane separation and caving of the roof. From these observations, it can be inferred that some of the parameters that affect the aperture of fractures at a longwall site are in-situ stress magnitudes and orientations, natural fracture geometries and apertures before mining, panel width, mining height, pillar dimensions, and mechanical properties of overburden rock layers. The orientation of natural and induced fractures with respect to the principal stresses and mining direction contribute to the stress concentration on fracture planes and thus their apertures. Panel and pillar geometries, the caving process, overburden deformations, and induced stresses are factors that can influence fracture apertures. Rock mechanical properties such as elastic modulus mainly define rock deformation and thus fracture apertures under a given stress level.

The stochastic DFN modeling approach replicates the variation of these parameters. However, for the objective of developing mitigation strategies, it is important to understand the impact of each fracture parameter on a potential gas flow to the mine. Therefore, this study utilizes a deterministic approach to develop a conceptualized DFN model that is representative of the typical fracture network in the overburden. This does not represent a real-world fracture network, but it is a simplified conceptual model that captures some of the important aspects of the problem, and it is used as a testbed to investigate the impact of select parameters. The parameters include fracture length, fracture aperture, fracture water saturation level, and methane generation in adjacent strata. For example, to investigate a parameter such as fracture length, a single fracture from the network is selected and the length is deterministically varied. A similar approach is used to study the impact of fracture aperture. To investigate the impact of water saturation, all the fractures in the network are assumed to be saturated with immobile water.

RESEARCH APPROACH

As described in the Introduction, a conceptualized DFN model is developed to conduct a parametric study on the influence of different parameters on shale gas flow to the mine in the event of a casing breach. Figure 2 shows a representation of the conceptualized DFN model with all the fracture ends numbered and identified as nodes. This is based on the approach presented by Priest [10] for flow through discontinuities and also used in a prior study by Ajayi and Schatzel [11]. The model shows 10 external nodes (1–10) along with 9 internal nodes (11–19).

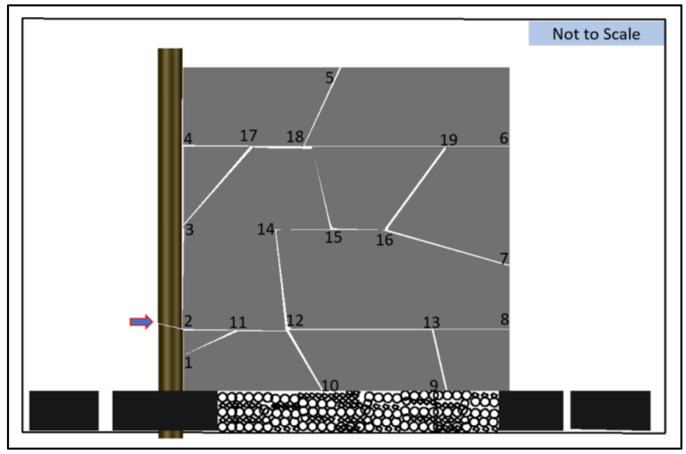

Figure 2. A representation of the conceptual/deterministic discrete fracture network (DFN) used for this study. The arrow indicates the breach location. Nodes 1-10 are external nodes of the fracture network and nodes 11-19 are internal nodes of the fracture network.

Impact of Overburden Gas Generation

At a study site in southwestern Pennsylvania, a geomechanical study observed lateral overburden movement (perpendicular to the direction of mining) of 17 cm (6.69 in) at the Sewickley coal horizon and 4 cm (1.57 in) at the Uniontown coal horizon in the overburden [12]. Meaning, the coal seams in the overburden are some of the most likely locations predicted for a casing breach, primarily along the interfaces between weak and strong strata. This is also dependent on distance between these interfaces and the mining horizon. If there is a breach at a stratum with in-situ gas generation, the induced pressure and concentration difference could also facilitate the transport of strata-generated gas such as methane. Ajayi and Schatzel [13] established that the gas flow trend could change due to the presence of gas generated along the fracture path. In order to investigate the impact of gas generation within the nearby strata, this study uses the equation derived by Ajayi and Schatzel [13] for gas flux, J ($kg/m^2 s$), through a single fracture [13]:

$$J(L) = \mu c_L - \Upsilon c_o + q\,\xi \tag{1}$$

In Equation 1,

$$\mu = \frac{u}{1 - e^{uL/D}},\ \Upsilon = \frac{u e^{uL/D}}{1 - e^{uL/D}},\ and\ \xi = q\left[L - \frac{L}{1 - e^{e^{uL/D}}} - \frac{D}{u_{i-j}}\right].$$

where u is the gas velocity (m/s), c is the gas concentration (kg/m^3), *D* is the gas diffusion coefficient through the medium (m^2/s), and q is the stratum's gas generation rate ($kg/m^3 s$). For a fracture of length, *L* (m), $c(0) = c_o$ and $c(L) = c_L$. q represents gas generation from the strata into the fracture or could be further described as gas flux per unit aperture from the wall of the fractures. The gas flow velocity, *u* in Equation 1, is derived from cubic law using the pressure heads derived in Equation 2.

$$u = -\frac{\rho g\, b^2}{12\,\mu\, L}\,\Delta H \tag{2}$$

ΔH is the pressure head difference between both nodes, ρ is the density of fluid (kg/m^3), L is the length of the fractures (m), b is the fracture aperture (m), g is the acceleration due to gravity (m/s^2), and μ is the dynamic viscosity (Ns/m^2). By applying mass balance at the internal nodes, a system of equations is formed as Equation 3 (see APPENDIX):

For ease of comparison on the impact of gas generation within the strata in the overburden, a dimensionless flux approach is developed by re-deriving Equation 1 into a dimensionless form using advection flux ($u\,c_\infty$):

$$J^*(L) = \left[\frac{c_L^* - c_o^*\, e^{\varphi_1 - \varphi_2}}{1 - e^{\varphi_1}}\right] + \varphi_2 - \frac{\varphi_2}{\varphi_1} \quad (4) \tag{4}$$

The dimensionless parameters in Equation 4 are:

$$\varphi_1 = \frac{uL}{D}, \tag{5}$$

$$\varphi_2 = \frac{q\,L}{u\,c_\infty}, \tag{6}$$

φ_1 is Peclet number, which is a parameter that characterizes transport due to advection compared to diffusion. φ_2 is derived for this study and defined as the Fract_gen number. c^* is a dimensionless shale gas concentration defined in this study as c/c_∞, where c_∞ is a fixed gas concentration that could be used to characterize the flow. For a specific site, c_∞ could be used to represent the maximum gas concentration at an infinite distance. However, for the purpose of this parametric study, no site-specific value is required.

Impact of Fracture and Gas Flow Parameters

This section discusses the method used to quantify the impact of shale gas pressure, fracture water saturation level, fracture length, and fracture aperture on shale gas flow to the mine using the defined fracture network in Figure 2. Gas flow through the fractures is modeled using cubic law:

$$Q = -\frac{\rho g\, b^3\, w}{12\,\mu\, L}\,\Delta H\,. \tag{7}$$

Here Q is the volume flow rate (m^3/s), and w is the fracture height assumed to be 1 m for this two-dimensional model. Several studies have predicted a critical Reynold's number (Re_c), beyond which the assumptions for cubic law are not sufficient and the flow could transition to nonlinear flow. This is highly dependent on the fracture roughness, and a range of 1-2300 has been derived for the critical Reynolds number with several upper limits within this range. Another study shows that the cubic law accurately predicted non-Darcian flow if inertial effects are limited and the fracture flows with the Forchheimer number are < 1.30 [14]. This is a subject that requires more research, but it is not the focus of this work. So, based on available information, the critical Reynold's number used for the validity of this model is 2300. Hence, it is expected that $Re_c < 2300$. Considering a unit fracture width, the critical pressure gradient (∇p_c) required to meet the 2300 critical Reynold's number is derived as:

$$\nabla p_c < \frac{2300 \times 12 \times \mu^2}{\rho\, b^3}. \tag{8}$$

For a mean aperture of $1 \times 10^{-4}\,m$ surrounding the pillar, the critical pressure gradient (∇p_c) for the methane model is $\approx 5.0909 \times 10^6\,Pa/m$. So, for a 5-m-long fracture, the critical pressure is $\approx 25.5\,MPa\,(3698\,psi)$. Therefore, the range of gas pressures considered in this study (2.4 MPa (350 psi) – 20.7 MPa (3000 psi)) is lower than the critical pressure. To predict the gas flow, mass conservation is applied at each of the internal fracture nodes with the assumptions that the pressure head at the boundary nodes is known while the internal nodes are unknown. Using the fracture network in Figure 2, the total gas flow to the mine is the sum of flow through fractures 12–10 and 13–9. Applying mass balance at the internal nodes:

$$Q_{i-j} = C_{i-j}\,(H_j - H_i), \tag{9}$$

where C_{i-j}, the fracture conductance is:

$$C_{i-j} = \frac{\rho g\, b_{i-j}^3\, w}{12\,\mu\, L_{i-j}} \tag{10}$$

Equation 11 (see APPENDIX) shows the system of equations derived by applying Equation 9 to the defined fracture network and used for predicting the pressure head of the internal nodes.

Where $d_{i-j} = C_{i-j}/C_{sj}$. C_{sj} is the sum of all conductance for fractures connecting to node j using the approach elucidated by Priest [10]. Fractures in the Northern Appalachian Basin are often saturated with water, which could have an impact on the gas flow. Kissell and Edwards [15] studied gas flow in coalbeds and observed that methane emission increases as the fracture water saturation level decreases. Therefore, this study investigates the impact of water saturation on gas flow to the mine. This is a two-phase flow model, but it is further simplified by assuming that the fractures are filled with immobile water. With this assumption, the water pressure head difference between the two fracture nodes is approximately zero and the water flow is zero ($Q_w = 0$). Based on this approach, the gas flow equation from the cubic law is expressed as:

$$Q_g = -\frac{\rho g\, b_g^3\, w}{12\,\mu\, L}\,\Delta H\,. \tag{12}$$

In Equation 12, b_g is the aperture value available for gas flow, and it is a fraction of the total fracture aperture. Table 1 presents the base parameters for the fracture network in Figure 2. Since methane is the main constituent of shale gas, the gas is modeled as methane with a density (ρ) of $0.656\,kg/m^3$ and dynamic viscosity (μ) of $1.01 \times 10^{-5}\,Ns/m^2$. The aperture used is assumed to be the effective hydraulic aperture which represents the aperture that will generate an equivalent flow with the same pressure gradient. Therefore, the impact of fracture convolutedness is assumed to be negligible.

Table 1. Summary of Fracture parameters for the Conceptualized DFN Model.

Node i	Node j	Length (m)	Aperture (m) Base Case
2	11	18.0	2.5×10^{-4}
12	11	8.0	6.0×10^{-4}
1	11	13.0	1.0×10^{-4}
10	12	15.9	4.0×10^{-3}
14	12	22.8	2.0×10^{-5}
13	12	17.5	6.5×10^{-4}
8	13	17.4	2.0×10^{-4}
9	13	14.2	1.0×10^{-3}
15	14	11.9	9.0×10^{-5}
18	15	13.0	1.0×10^{-5}
16	15	11.9	9.0×10^{-5}
7	16	29.7	9.0×10^{-5}
19	16	22.5	1.0×10^{-5}
3	17	13.0	1.0×10^{-5}
4	17	15.5	1.0×10^{-5}
18	17	12.3	1.0×10^{-5}
5	18	20.0	8.0×10^{-6}
19	18	29.6	1.0×10^{-5}
18	19	29.6	1.0×10^{-5}
6	19	15.3	1.0×10^{-5}

RESULTS AND DISCUSSION

This section discusses the results of the impact of flow parameters on shale gas transport to the mine using the conceptualized/deterministic DFN model in Figure 2. The impact of gas generation along the flow path is studied using a dimensionless flux approach as described in Section 2.1. The two dimensionless numbers derived in Equations 5 and 6 could be calculated for each fracture length in Figure 2. The dimensionless number used to quantify gas generation along the fracture path is the Fract_gen number in Equation 6. From the defined fracture network in Figure 2, the impact of gas generation along fracture 11 to 12 is investigated. The Fract_gen number is varied by only changing the gas generation rate (q) in Equation 6. Figure 3 shows the plot of the dimensionless flux with Fract_gen number along fracture 11-12. The plot shows that the gas flux is very sensitive to the Fract_gen number. An increase in the Fract_gen number increases the dimensionless flux. A 50% increase in the Fract_gen number, as indicated in Figure 3, could increase the dimensionless flux up to 30%. This implies that the flow of shale gas through the fracture network could further enhance the transport of gases generated within the fracture network. It also indicates that a similar breach could result in a different volume of gas flow to the mine based on the geology of the site.

The pressure of shale gas in the casing is dependent on several operating conditions. The operating pressures of most unconventional shale gas wells in the Northern Appalachian Basin are between 1.03 to 2.41 MPa (150 to 350 psi). In an event where the gas well is shut in for repairs or any emergency, the gas pressure builds rapidly up to 20.68 MPa (3,000 psi). Therefore, the impact of the gas pressure is investigated along with the water saturation level as shown in Figure 4. It is observed that the gas flow decreases with an increase in the water saturation level in the fractures. From the results, a 100% increase in the water saturation level could decrease the potential gas flow by 30–70% as summarized in Table 2. This shows that the presence of immobile water in the fractures could help to limit the gas flow. These results further support the previous findings on the implications of relative permeability with respect to methane transport in mines by Kissell and Edward [15]. They observed that a drainage hole drilled into the working face of a mine emitted 7,260 ft^3/day of methane and 72 gal/day of water for several days. However, on the sixth day, the water level decreased to 48 gal/day, and the methane flow rate increased to 7,960 ft^3/day. Similarly, Zabetakis observed that methane permeability for an older rib was higher than a freshly exposed rib due to a decrease in the coal rib water content [16].

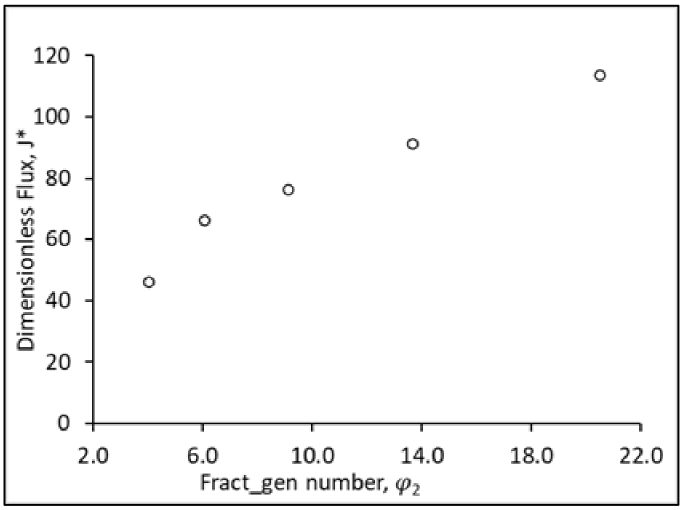

Figure 3. Plot of dimensionless flux with Fract_gen number.

Table 2. Analysis of the Impact of Fracture Saturation Level.

Water Saturation Level (%)	*Approximate Gas Flow Percentage Change (%)*
10–20	30
20–40	58
25–50	70

Therefore, potential gas flow to the mine could be higher if the breach occurs several months after mining (though not anticipated) due to a decrease in the fracture water content. Figure 4 also shows the impact of varying gas pressure on gas flow. At 0% water saturation, the gas flow rates are 32 cfm, 93 cfm, and 278 cfm for 2.41 MPa (350 psi), 6.89 MPa (1,000 psi), and 20.68 MPa (3,000 psi) gas pressure, respectively. A 185% increase in the pressure from 2.41 MPa (350 psi) to 6.89 MPa (1,000 psi) increased the gas flow also by 185% (≈32 cfm to ≈93 cfm). Also, a 200% increase in pressure from 6.89 MPa (1,000 psi) to 20.68 MPa (3,000 psi) increases the gas flow by approximately 200% (≈93 cfm to ≈278 cfm). This implies that under the same flow conditions, a change in the pressure will generate a corresponding change in the gas flow.

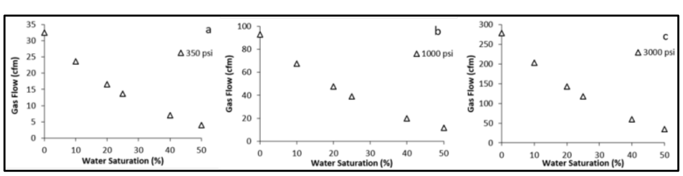

Figure 4. Variation in gas flow with water saturation level.

Gas flow through the fractures is modeled with the cubic law in Equation 12. From Equation 12, the aperture value has a power of 3, which shows that the gas flow is highly sensitive to changes in the fracture aperture. Therefore, using the defined DFN model in Figure 2 along with the base values in Table 1, the impact of aperture variation on the gas flow is investigated. From Figure 2, one of the critical aperture values is the fracture directly connected to the breached casing between nodes 2–11. This investigation is conducted using a production pressure of 350 psi and a 25% immobile fracture water saturation. Figure 5 shows a plot of the gas flow with the aperture value at the breach location (nodes 2–11 in Figure 2). The result shows that the gas flow increases significantly as the aperture value increases. A 100% increase in the aperture of the fracture connected to the casing from 1×10^{-4} m to 2×10^{-4} m increased the gas flow from 0.9 cfm to 7.12 cfm, approximately a 689% increase. Similarly, a 100% increase in the aperture from 2.4×10^{-4} m to 4.8×10^{-4} m increased the gas flow from 12.17 cfm to 81.50 cfm, about a 570% increase in the gas flow. This also implies that a 100% reduction in the fracture aperture could reduce the gas flow in a similar proportion. Therefore, the aperture of fractures near the casing is one of the most critical parameters that determines the likelihood of gas migrating from a breached casing toward the mine. Hence, recommendations to proactively mitigate shale gas flow to the mine (in the event of a casing breach) should consider measures to ensure the fracture aperture at the center of the pillar (where the casing is positioned) is as low as possible. As highlighted in the Introduction, some of the mine design parameters that could influence the fracture aperture are the panel width, mining height, and pillar dimensions.

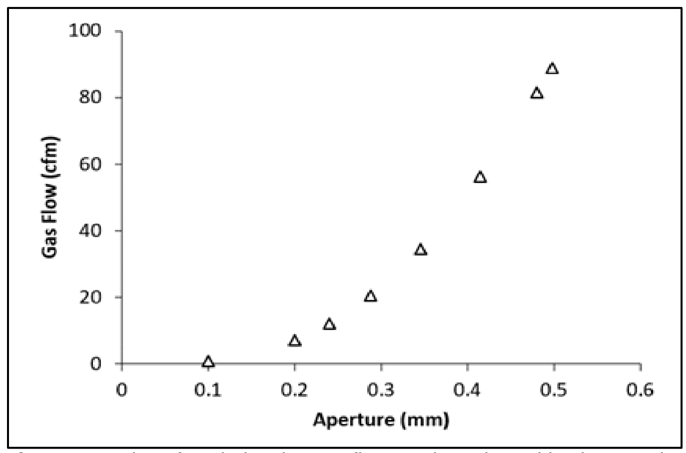

Figure 5. Plot of variation in gas flow to the mine with changes in aperture of fracture connected to the casing breach (node 2 in Figure 2).

In Figure 2, the fracture distance from node 2 to node 11 could be regarded as the setback distance, the distance from the location of the gas well in the pillar to the edge of the panel and is related to the pillar dimensions or drill pattern. In the base values for the fracture network presented in Table 1, the fracture length is 18 m. At a study site in Southwestern PA, the size of the abutment pillar is 38.1 m × 83.82 m (125 ft × 275 ft) [7]. Assuming the well is positioned at the center of the pillar, the 18-m fracture length is quite representative of the study site's setback distance. To understand the impact of this dimension, Figure 6 shows the plot of gas flow to the mine with respect to changes in the fracture length between nodes 2 to 11, which could also be classified as a bedding plane. It is observed that the gas flow decreases with an increase in the fracture length due to the pressure loss as the gas travels through the fracture network. In reality, changing the dimensions of the pillar could affect the aperture size, but for this study the apertures are assumed to be constant for all fracture lengths. With this assumption, a 100% increase in the fracture length from the breach location (nodes 2–11) from 9 m to 18 m decreased the gas flow to the mine by about 48% from 26.57 cfm to 13.7 cfm. It is likely that the changes could be more significant if the impact of the pillar dimension on the aperture is incorporated. However, this study shows that the gas flow to the mine could be reduced by the setback distance. Therefore, for deeper cover, where it is anticipated that the pillar dimensions could be larger, the gas flow to the mine could be lower.

According to most of the pillar design methods, the depth of cover has a great effect on the size of the pillar. For example, the Choi and McCain formula suggests a 4-times increase in the pillar dimension for a mine depth increase from 152.4 m (500 ft) to 609.6 m (2,000 ft) [17].

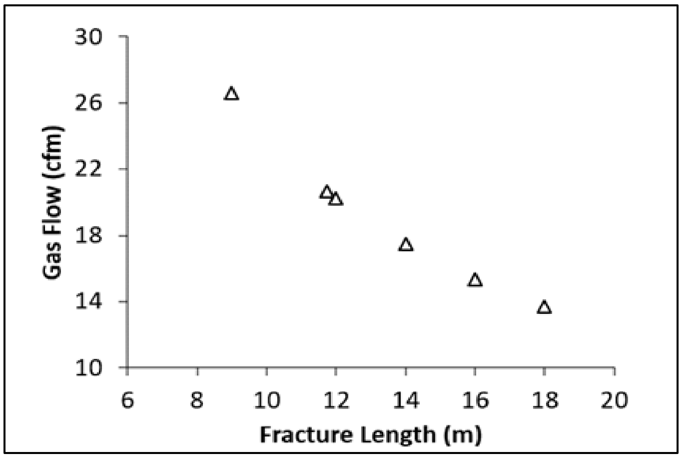

Figure 6. Plot of gas flow to the mine with variation in fracture length from breach sources (nodes 2–11 in Figure 2 and Table 1).

CONCLUSIONS

This study focuses on predicting the impact of parameters that could affect gas flow to the mine in the event of a shale gas well casing breach. Instead of using a stochastic approach, a conceptualized/deterministic DFN model is used to investigate the effect of each parameter with the intent of understanding the isolated impact of each parameter. A dimensionless approach is used to investigate the impact of gas generation along the fracture network using a methodology developed in this study. The findings show that:

i. Methane generation along the fracture network could significantly change the overall gas flux to the mine. Hence, it is likely that a similar casing breach could generate different gas fluxes if there is a gas-bearing stratum along the flow pathway.
ii. The presence of immobile water in the fracture reduces the risk of gas flow to the mine by decreasing the proportion of the fracture aperture that is available for gas flow.
iii. Under the same flow condition, a change in the gas pressure directly affected the overall gas flow in the same proportion.
iv. The aperture of the fracture directly connected to the casing breach is a very critical parameter that significantly influences the gas flow from the breach location. Hence, it is suggested that the coal pillars where gas wells are positioned should be designed to minimize the aperture of mining-induced fractures near the well casing. Similarly, the distance from the position of the gas well casing to the edge of the panel has an impact on the potential gas flow.

Overall, these findings provide critical information that could contribute to the development of guidelines to proactively mitigate potential shale gas flow to the mine in the event of a casing breach.

DISCLAIMER

The findings and conclusions in this report are those of the authors and do not necessarily represent the official position of the National Institute for Occupational Safety and Health, Centers for Disease Control and Prevention. Mention of any company or product does not constitute endorsement by NIOSH.

REFERENCES

1. Zhang, P., D. Su, and J. Lu. *Influence of Longwall Mining on the Stability of Shale Gas Wells in Barrier Pillars*. in *American Rock Mechanics Association*. 2019. New York.

2. Commonwealth of Pennsylvania *Joint Coal and Gas Committee, Gas Well Pillar Study*, Department of Mines and Mineral Industries Oil and Gas Division, Editor. 1957: Harrisburg, Pennsylvania: . p. 28 pp.

3. Pennsylvania Department of Environmental Protection. *Longwall mine data*. [cited 2021 09/29]; Available from: https://www.dep.state.pa.us/dep/deputate/minres/LongwallForestlandStudy/Table1.pdf.

4. Berryhill, H.L., *Coal Reserves of the Pittsburgh (no. 8) Bed in Belmont County, Ohio*. 1955.

5. Schatzel, S.J., C.Ö. Karacan, H. Dougherty, and G.V. Goodman, *An analysis of reservoir conditions and responses in longwall panel overburden during mining and its effect on gob gas well performance.* Engineering Geology, 2012. **127**: p. 65-74.

6. Doolin, D. and M. Mauldon, *Fracture permeability normal to bedding in layered rock masses.* International Journal of Rock Mechanics and Mining Sciences, 2001. **38**(2): p. 199-210.

7. Ajayi, K., Z. Khademian, S. Schatzel, E. Watkins, and V. Gangrade, *Numerical modeling of longwall-induced permeability under shallow cover*, in *Mine Ventilation*. 2021, CRC Press. p. 389-397.

8. Watkins, E., C.Ö. Karacan, V. Gangrade, and S. Schatzel, *Assessing Gas Leakage Potential into Coal Mines from Shale Gas Well Failures: Inference from Field Determination of Strata Permeability Responses to Longwall-Induced Deformations.* Natural Resources Research, 2021: p. 1-14.

9. Khademian Z., K.M. Ajayi, D.W.H. Su, G. Esterhuizen, and S.J. Schatzel. *Geomechanical modeling of mining-induced permeability: implications for potential gas inflow from a sheared gas well*. 2021. Canonsburg, PA.

10. Priest, S.D., *Fluid Flow in Discontinuities*, in *Discontinuity analysis for rock engineering*. 2012, Springer Science & Business Media.

11. Ajayi, K.M. and S.J. Schatzel, *Transport model for shale gas well leakage through the surrounding fractured zones of a longwall mine.* International Journal of Mining Science and Technology, 2020.

12. Su, D., P. Zhang, H. Dougherty, M. Van Dyke, T. Minoski, S. Schatzel, V. Gangrade, E. Watkins, J. Addis, and C. Hollerich. *Longwall-Induced Subsurface Deformations and Permeability Changes—Shale Gas Well Casing Integrity Implication*. in *Proceedings of the 38th International Conference on Ground Control in Mining*. 2019. Society for Mining, Metallurgy & Exploration.

13. Ajayi, K.M. and S.J. Schatzel, *Transport model for shale gas well leakage through the surrounding fractured zones of a longwall mine.* International Journal of Mining Science and Technology, 2020. **30**(5): p. 635-641.

14. Ranjith, P. and D. Viete, *Applicability of the 'cubic law'for non-Darcian fracture flow.* Journal of Petroleum Science and Engineering, 2011. **78**(2): p. 321-327.

15. Kissell, F.N. and J.C. Edwards, *Two-phase flow in coalbeds.* 1975.

16. Zabetakis, M.G., *Methane emission in coal mines: effects of oil and gas wells*. Vol. 7658. 1972: US Department of Interior, Bureau of Mines.

17. Mark, C., *Pillar design methods for longwall mining*. Vol. 9247. 1990: US Department of the Interior, Bureau of Mines.

APPENDIX

$$\begin{pmatrix} \begin{pmatrix} \mu_{1-11}+ \\ \mu_{2-11}+ \\ \mu_{12-11} \end{pmatrix} & -\gamma_{12-11} & 0 & 0 & 0 & 0 & 0 & 0 & 0 \\ -\gamma_{11-12} & \begin{pmatrix} \mu_{10-12}+ \\ \mu_{11-12} \\ +\mu_{14-12} \\ +\mu_{13-12} \end{pmatrix} & -\gamma_{13-12} & -\gamma_{14-12} & 0 & 0 & 0 & 0 & 0 \\ 0 & -\gamma_{12-13} & \begin{pmatrix} \mu_{8-13}+ \\ \mu_{9-13} \\ +\mu_{12-13} \end{pmatrix} & 0 & 0 & 0 & 0 & 0 & 0 \\ 0 & -\gamma_{12-14} & 0 & \begin{pmatrix} \mu_{12-14} \\ +\mu_{15-14} \end{pmatrix} & -\gamma_{15-14} & 0 & 0 & 0 & 0 \\ 0 & 0 & 0 & -\gamma_{14-15} & \begin{pmatrix} \mu_{14-15}+ \\ \mu_{16-15} \\ +\mu_{18-15} \end{pmatrix} & -\gamma_{16-15} & 0 & -\gamma_{18-15} & 0 \\ 0 & 0 & 0 & 0 & -\gamma_{15-16} & \begin{pmatrix} \mu_{7-16} \\ +\mu_{15-16} \\ +\mu_{19-16} \end{pmatrix} & 0 & 0 & -\gamma_{19-16} \\ 0 & 0 & 0 & 0 & 0 & 0 & \begin{pmatrix} \mu_{3-17} \\ +\mu_{4-17} \\ +\mu_{18-17} \end{pmatrix} & -\gamma_{18-17} & 0 \\ 0 & 0 & 0 & 0 & -\gamma_{15-18} & 0 & -\gamma_{17-18} & \begin{pmatrix} \mu_{5-18} \\ +\mu_{15-18} \\ +\mu_{17-18} \\ +\mu_{19-18} \end{pmatrix} & -\gamma_{19-18} \\ 0 & 0 & 0 & 0 & 0 & -\gamma_{16-19} & 0 & -\gamma_{18-19} & \begin{pmatrix} \mu_{6-19} \\ +\mu_{16-19} \\ +\mu_{18-19} \end{pmatrix} \end{pmatrix} \begin{pmatrix} c_{11} \\ c_{12} \\ c_{13} \\ c_{14} \\ c_{15} \\ c_{16} \\ c_{17} \\ c_{18} \\ c_{19} \end{pmatrix} = \begin{pmatrix} \begin{bmatrix} -\xi_{1-11}-\xi_{2-11}- \\ \xi_{12-11}+\gamma_{1-11}c_1 \\ +\gamma_{2-11}c_2 \end{bmatrix} \\ \begin{bmatrix} -\xi_{10-12}-\xi_{11-12}- \\ \xi_{13-12}-\xi_{14-12} \\ +\gamma_{10-12}c_{10} \end{bmatrix} \\ \begin{bmatrix} -\xi_{8-13}-\xi_{9-13}- \\ \xi_{12-13}+\gamma_{8-13}c_8 \\ +\gamma_{9-13}c_9 \end{bmatrix} \\ \left[-\xi_{12-14}-\xi_{15-14}\right] \\ \begin{bmatrix} -\xi_{14-15}-\xi_{16-15} \\ -\xi_{18-15} \end{bmatrix} \\ \begin{bmatrix} -\xi_{7-16}-\xi_{15-16} \\ -\xi_{19-16}+\gamma_{7-16}c_7 \end{bmatrix} \\ \begin{bmatrix} -\xi_{3-17}-\xi_{4-17} \\ -\xi_{18-17} \\ +\gamma_{3-17}c_3+\gamma_{4-17}c_4 \end{bmatrix} \\ \begin{bmatrix} -\xi_{5-18}-\xi_{15-18}- \\ \xi_{17-18}-\xi_{19-18} \\ +\gamma_{5-18}c_5 \end{bmatrix} \\ \begin{bmatrix} -\xi_{6-19}-\xi_{16-19} \\ -\xi_{18-19}+\gamma_{6-19}c_6 \end{bmatrix} \end{pmatrix} \quad (3)$$

$$\begin{bmatrix} -1 & d_{12-11} & 0 & 0 & 0 & 0 & 0 & 0 & 0 \\ d_{11-12} & -1 & d_{13-12} & d_{14-12} & 0 & 0 & 0 & 0 & 0 \\ 0 & d_{12-13} & -1 & 0 & 0 & 0 & 0 & 0 & 0 \\ 0 & d_{12-14} & 0 & -1 & d_{15-14} & 0 & 0 & 0 & 0 \\ 0 & 0 & 0 & d_{14-15}\,H_{14} & -1 & d_{16-15} & 0 & d_{18-15} & 0 \\ 0 & 0 & 0 & 0 & d_{15-16}\,H_{15} & -1 & 0 & 0 & d_{19-16} \\ 0 & 0 & 0 & 0 & 0 & 0 & -1 & d_{18-17} & 0 \\ 0 & 0 & 0 & 0 & d_{15-18} & 0 & d_{17-18} & -1 & d_{19-18} \\ 0 & 0 & 0 & 0 & 0 & d_{16-19} & 0 & d_{18-19} & -1 \end{bmatrix} \begin{bmatrix} H_{11} \\ H_{12} \\ H_{13} \\ H_{14} \\ H_{15} \\ H_{16} \\ H_{17} \\ H_{18} \\ H_{19} \end{bmatrix} = \begin{bmatrix} -d_{2-11}\,H_2 - d_{1-11}\,H_1 \\ -d_{10-12}\,H_{10} \\ -d_{9-13}\,H_9 - d_{8-13}\,H_8 \\ 0 \\ 0 \\ -d_{7-16}\,H_7 \\ -d_{4-17}\,H_4 - d_{3-17}\,H_3 \\ -d_{5-18}\,H_5 \\ -d_{6-19}\,H_6 \end{bmatrix} \quad (11)$$